# Seamless elastic boundaries for atomistic calculations

Lars Pastewka,[1,2,*] Tristan A. Sharp,[1] and Mark O. Robbins[1,†]

[1]*Department of Physics and Astronomy, Johns Hopkins University, 3400 North Charles Street, Baltimore, Maryland 21218, USA*

[2]*MikroTribologie Centrum μTC, Fraunhofer-Institut für Werkstoffmechanik IWM, Wöhlerstraße 11, D-79108 Freiburg, Germany*

(Received 19 June 2012; revised manuscript received 27 July 2012; published 27 August 2012)

Modeling interfacial phenomena often requires both a detailed atomistic description of surface interactions and accurate calculations of long-range deformations in the substrate. The latter can be efficiently obtained using an elastic Green's function if substrate deformations are small. We present a general formulation for rapidly computing the Green's function for a planar surface given the interatomic interactions, and then coupling the Green's function to explicit atoms. The approach is fast, avoids ghost forces, and is not limited to nearest-neighbor interactions. The full system comprising explicit interfacial atoms and an elastic substrate is described by a single Hamiltonian and interactions in the substrate are treated exactly up to harmonic order. This concurrent multiscale coupling provides simple, seamless elastic boundary conditions for atomistic simulations where near-surface deformations occur, such as nanoindentation, contact, friction, or fracture. Applications to surface relaxation and contact are used to test and illustrate the approach.

DOI: 10.1103/PhysRevB.86.075459 PACS number(s): 68.35.Gy, 62.20.D−, 46.25.Cc, 46.55.+d

## I. INTRODUCTION

A large number of interfacial problems are challenging to simulate using brute-force methods. The response depends on details of atomic interactions at the interface and also on long-range elastic deformations of the bulk. This situation arises in studies of contact and friction in scanning probe experiments[1,2] or between atomically rough surfaces,[3,4] and fracture of brittle[5] or ductile[6] materials. The elastic response of the supporting solid can also appreciably influence chemi- and physisorption processes at crystal surfaces, including stress corrosion[7] and thin-film growth.[8]

There has been great recent interest in accelerating such simulations by treating each spatial region with the modeling method that most efficiently captures material response.[5–7,9–12] An explicit atomistic treatment is essential at the interface where gradients in stress, strain, and chemical composition may be large. Long-range elastic deformations in the bulk extend to depths that are comparable to the length scale of variations along the interface $L$, but the strains at these depths may be small enough to treat with models that assume slow variations and/or linear response. In many cases, a simplified treatment of the substrate may decrease the computational cost for force calculations substantially, from order $L^3$ to order $L^2 \ln(L)$.

A variety of methods for approximating the response of the substrate have been proposed and many are reviewed and contrasted in Refs. 9 and 11. Most treat the interface atomistically and transition to a finite-element description for the bulk. In general, this introduces ghost forces near the interface or leads to a model with no underlying Hamiltonian.[9,12] There is an alternative approach that avoids both problems. An atomistic description is retained throughout the system, but atomic interactions in the substrate are treated in the harmonic approximation. The linear response of the substrate can then be efficiently calculated using Green's function methods.

Traditionally, Green's function techniques have been used to describe the elastic response of the infinite or semi-infinite bulk to inclusions such as point, line, or planar defects by invoking the Dyson equation.[13–16] Recent extensions of this approach have included a full nonlinear atomistic description of the defect coupled to a harmonic lattice[17] that smoothly connected to a continuum description at large distances.[18–20] Green's function techniques have also been employed to solve boundary value problems in continuum elasticity.[21–23] An atomistic system can be coupled to a continuum boundary,[20,24] but the strain field will only match exactly for long-wavelength deformations. Recently, Campaña and Müser[25] showed that a Green's function approach can be used for the solution of atomic-scale contact problems. In their work, the surface Green's function is evaluated from a fluctuation-dissipation theorem. Assuming that the underlying potential is harmonic, the mean response is not affected by these fluctuations. A similar method was used to find the dynamic Green's function in complex geometries by Cai *et al.*[26] Most applications of the Green's function approach to atomic scale contact problems[4,25,27–29] have used the analytic solution[30] for simple cubic lattices or the isotropic continuum Green's function.[3,31] An implementation of the code has been ported to the widely used molecular dynamics package LAMMPS.[32–34]

There are two difficulties with the Green's function approach as it has been implemented for atomic scale contact problems. One is that the formulation does not include all the atomic forces near the interface between explicit and harmonic regions. The neglected forces vanish in the special case of nearest-neighbor interactions at zero pressure, which has been considered in most past work. In other cases, these forces must be included or the coupled system does not satisfy Newton's third law. Neglecting them creates problems similar to ghost forces in other methods[9] and creates artificial surface relaxation at the elastic/explicit interface. The second difficulty is that calculating the Green's function with the fluctuation dissipation theorem can require significant computation. All $L^3$ atoms in the substrate must be included and sampling long-wavelength modes correctly requires times that are at least of order $L$.[35] Thus, while the Green's function needs to be calculated only once, it may require more computational effort than calculations using it.

 

In this paper we describe an approach that includes all interatomic forces near the interface and allows rapid calculation of the elastic Green's function for an arbitrary interaction. Fourier transforming the equations of motion in the plane of the substrate decouples the equations for each in-plane wave vector $\vec{q}$.[36] The remaining coupling between atomic planes of the substrate is effectively one dimensional and can be solved for any crystalline solid without the need of separate molecular dynamics simulations and fluctuation/dissipation analysis. Prescriptions for solving the equations using a transfer matrix formulation[36,37] and a renormalization transformation[38,39] are described. Full dynamical equations are developed for a number of crystals and interactions and then implemented for static problems. The static Green's function can be precomputed in a time that is $O(L^2 \ln L)$ and, thus, represents a negligible fraction of the total computation time for contact problems. The only approximation intrinsic to this construction is linear response sufficiently far below the surface.

To demonstrate that the resulting approach provides seamless boundary conditions for interfacial calculations we apply the method to three cases (Sec. III). The first is relaxation of the spacing between atomic planes near a free surface. Full atomistic results are reproduced by our method, but previous formulations do not include the forces that produce surface relaxation.[25,33] We next consider Hertzian contact between a rigid sphere and elastic substrate and show that a few planes of explicit atoms on the Green's function layer allow the anharmonic corrections to Hertz theory to be captured. Our last example is contact of a randomly rough stepped surface with a flat substrate. A few planes of explicit atoms allow both anharmonic effects and subsurface plasticity to be captured up to relatively high contact areas.

## II. ELASTIC SURFACE GREEN'S FUNCTIONS

We start from the total energy $E(\{\vec{r}_{i\alpha}\})$ of the crystal as a function of the positions of all atoms $\vec{r}_{i\alpha}$. The energy may have arbitrary form and could be replaced by the free energy to model the response at finite temperature. Atoms are then partitioned into three types (see Fig. 1): substrate atoms, boundary atoms, and explicit atoms. The explicit atoms may be anything that interacts with the boundary atoms, including a continuation of the crystal, adsorbed atoms, or atoms from an opposing surface. The goal of the Green's function formulation is to absorb the linear response of the substrate atoms into an effective interaction between boundary atoms. This reduces the total number of degrees of freedom to those of the boundary and explicit atoms.

The width of the boundary region must be greater than the range of interactions so there are no direct interactions between explicit and substrate atoms. The boundary layer is constructed so it satisfies this condition and contains an integer number of primitive unit cells along its width. The substrate is then divided into layers of the same width, so all atoms are accounted for and each layer only interacts with adjacent layers. In the following, Greek indices $\alpha, \beta, \ldots$ identify layers, with the boundary layer at $\alpha = 0$ (see Fig. 1). Latin indices $i$, $j, \ldots$ will number unit cells within each of these layers.

The total energy is divided into terms that involve interactions between explicit atoms, $E_{\mathrm{ee}}$, between explicit and boundary atoms, $E_{\mathrm{eb}}$, and between boundary or substrate atoms, $E_{\mathrm{bs}}$,

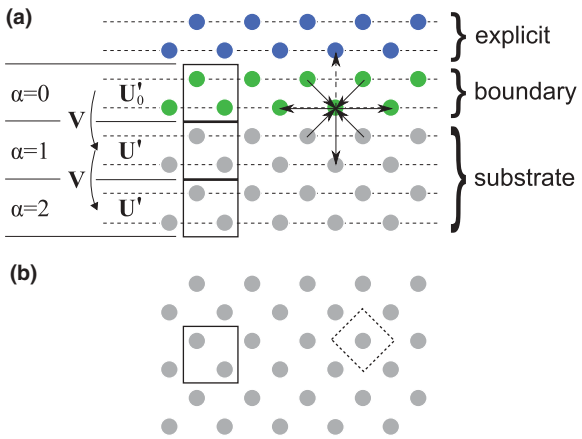


FIG. 1. (Color online) (a) Side view of a face-centered cubic (fcc) crystal with a (100) surface showing the layer structure for second-nearest-neighbor interactions. The top atoms are treated explicitly. In this case, they represent a continuation of the crystal. The boundary layer ($\alpha = 0$) is thick enough to prevent direct interactions between explicit and substrate atoms. The effect on boundary atoms from the elastic response of substrate atoms is captured using the Green's function. The force-constant matrix $\mathbf{D}$ has diagonal components $\mathbf{U}'_0$ and $\mathbf{U}'$ within the layers and off-diagonal components $\mathbf{V}$ coupling adjacent layers. Layers are labeled by the index $\alpha$ and unit cells in each layer (square boxes) by the index $i$. Arrows show the atoms that produce a force on one atom in the boundary layer. Only the atoms in the boundary and substrate (solid arrows) contribute to the net elastic force $\vec{f}_{i0}$. As a result, there is a net force that would be balanced by the force from explicit atoms (dashed arrow) if the explicit atoms continued the fcc crystal. (b) Top view of atoms at top of boundary layer. Periodicity in this plane is used to decouple the response at different wave vectors in the first Brillouin zone of the crystal. The solid and dashed lines show the conventional and primitive unit cells for the surface.

$$E_{\mathrm{tot}} = E_{\mathrm{ee}} + E_{\mathrm{eb}} + E_{\mathrm{bs}}. \tag{1}$$

The first two terms are treated exactly, while $E_{\mathrm{bs}}$ is treated in the usual harmonic approximation.[17,40] The energy $E_{\mathrm{bs}}$ is expanded in terms of displacements about a reference configuration. This is usually the ground state but could be a crystal under a uniform strain that most closely approximates the loaded crystal. For example, under high contact pressures there will be a mean compressive strain that extends throughout the substrate.

We will denote the set of displacements from equilibrium for the $n_c$ atoms in unit cell $i$ in layer $\alpha$ by the $3n_c$ dimensional vector $\vec{u}_{i\alpha}$ (see also Appendix A). The harmonic approximation for $E_{\mathrm{bs}}$ can then be written as

$$E_{\mathrm{bs}} = E_0 - \sum_{i\alpha} \vec{f}_{i\alpha} \cdot \vec{u}_{i\alpha} + \frac{1}{2} \sum_{i\alpha j\beta} \vec{u}_{i\alpha} \mathbf{D}_{i\alpha j\beta} \vec{u}_{j\beta} + \mathcal{O}(u^3), \tag{2}$$

where $E_0$ is the energy of the reference state, $\vec{f}_{i\alpha}$ is a $3n_c$-dimensional vector giving the force on atoms in the $i\alpha$ unit

cell, and $\mathbf{D}_{i\alpha j\beta}$ is the $3n_c \times 3n_c$ force-constant matrix,

$$\mathbf{D}_{i\alpha j\beta} \equiv \left.\frac{\partial^2 E_{\rm bs}}{\partial \vec{u}_{i\alpha}\partial \vec{u}_{j\beta}}\right|_{\vec{u}_{i\alpha}=0,\vec{u}_{j\beta}=0}. \tag{3}$$

Since we expand about a static solution, the total force

$$\vec{f}_{i\alpha} \equiv -\left.\frac{\partial E_{\rm bs}}{\partial \vec{u}_{i\alpha}}\right|_{\vec{u}_{i\alpha}=0} \tag{4}$$

must vanish for all substrate atoms ($\alpha > 0$). For boundary atoms, $\vec{f}_{i0}$ is generally not zero because it includes only the boundary and substrate interactions. These are indicated by solid arrows in Fig. 1(a), and the forces coming from explicit atoms are indicated by dashed arrows. In this figure, the explicit atoms continue the ideal crystal and exert a force that is equal and opposite $\vec{f}^{\rm exp}_{i0} = -\vec{f}_{i0}$. If the crystal is terminated at the boundary layer, the unbalanced forces give rise to the well-known phenomena of surface relaxation.[41] Previous applications of Green's functions to contact mechanics[25] did not include $\vec{f}_{i0}$. However, they generally focused on nearest-neighbor interactions and crystals at zero pressure. For this very special case $\vec{f}_{i0}$ vanishes and there is no surface relaxation. In almost all other cases the forces must be included.

The dynamical equation for the boundary and substrate atoms can now be written as

$$\mathbf{m}\frac{\partial^2 \vec{u}_{i\alpha}}{\partial t^2} + \sum_{j\beta}\mathbf{D}_{i\alpha j\beta}\vec{u}_{j\beta} = \delta_{0\alpha}\left(\vec{f}_{i0} + \vec{f}^{\rm exp}_{i0}\right), \tag{5}$$

where $\mathbf{m}$ is a diagonal matrix whose elements equal the mass associated with each degree of freedom in the unit cell, the forces are only nonzero for the boundary layer, and $\vec{f}^{\rm exp}_{i0}$ is the force from explicit atoms. Note that even if explicit crystalline atoms are present on top of the boundary layer, the forces $\vec{f}_{i\alpha}$ and $f^{\rm exp}_{i\alpha}$ do not vanish individually and, hence, we need to consider both explicitly.

The dynamical equation is simplified by transforming into reciprocal space within the plane of the layers and remaining in real space in the perpendicular direction. Because the crystal retains translational symmetry within the plane [Fig. 1(b)], the equations for each two-dimensional wave vector $\vec{q}$ in the first Brillouin zone (BZ) are decoupled. We denote the set of two-dimensional lattice vectors that connect the unit cells within the boundary layer by $\vec{R}_{i0}$. The unit cells in all other layers are then located at $\vec{R}_{i\alpha} = \vec{R}_{i0} + \alpha\vec{c}$, where $\vec{c}$ is the basis vector connecting unit cells in adjacent layers. The Fourier transforms in space and time are defined as

$$\vec{u}_\alpha(\vec{q},\omega) = \sum_j \int_{-\infty}^{\infty} dt \vec{u}_{j\alpha}(t)e^{-i\vec{q}\cdot\vec{R}_{j0}+i\omega t}, \tag{6}$$

$$\vec{u}_{j\alpha}(t) = \int_{\rm BZ}\frac{d^2q}{A_{\rm BZ}}\int_{-\infty}^{\infty}\frac{d\omega}{2\pi}\vec{u}_\alpha(\vec{q},\omega)e^{i\vec{q}\cdot\vec{R}_{j0}-i\omega t}, \tag{7}$$

where the sum in the first equation is over all unit cells in the boundary layer. The integral in the second equation runs over all wave vectors in the two-dimensional first BZ of the surface and $A_{\rm BZ} = \int_{\rm BZ} d^2q$ is the BZ area.

Translational symmetry in the substrate guarantees that $\mathbf{D}_{i\alpha j\beta}$ depends only on relative positions $R_{i0} - R_{j0}$ and $\beta - \alpha$. The Fourier transform is

$$\mathbf{D}_{\beta-\alpha}(\vec{q}) = \sum_k \mathbf{D}_{j\alpha k\beta}e^{-i\vec{q}\cdot(\vec{R}_{j0}-\vec{R}_{k0})} \tag{8}$$

and must vanish for $|\beta - \alpha| > 1$ because interactions do not extend beyond adjacent layers. The convolution theorem can be used to write the Fourier transform of the dynamical equation [Eq. (5)] as

$$\sum_\beta(-\mathbf{m}\omega^2\delta_{\alpha\beta} + \mathbf{D}_{\alpha\beta}(\vec{q}))\vec{u}_\beta(\vec{q},\omega) = \delta_{\alpha 0}\vec{f}_{\rm tot}(\vec{q},\omega), \tag{9}$$

where $\vec{f}_{\rm tot}$ includes both internal and explicit forces and only acts on the boundary layer.

In the following we assume that the substrate terminates at layer $\alpha = N$. Within the substrate, $\mathbf{D}$ only depends on $\beta - \alpha$ and only couples adjacent layers. Let $\mathbf{U}'(\vec{q}) = \mathbf{D}_{\alpha\alpha}(\vec{q})$ be the force-constant matrix that couples within each layer and $\mathbf{V}_\alpha(\vec{q}) = \mathbf{D}_{\alpha(\alpha+1)}(\vec{q})$ the matrix coupling to the nearest layer beneath. Then $\mathbf{V}^\dagger_\alpha(\vec{q})$ is the matrix coupling to the nearest layer above (see Fig. 1), where $\dagger$ denotes the Hermitian conjugate. The force-constant matrix has a tridiagonal form that facilitates solution

$$\mathbf{D} = \begin{pmatrix} \mathbf{U}'_0 & \mathbf{V} & 0 & \cdots & 0 & 0 \\ \mathbf{V}^\dagger & \mathbf{U}' & \mathbf{V} & \cdots & 0 & 0 \\ 0 & \mathbf{V}^\dagger & \mathbf{U}' & \cdots & 0 & 0 \\ \vdots & \vdots & \vdots & \ddots & \vdots & \vdots \\ 0 & 0 & 0 & \cdots & \mathbf{U}' & \mathbf{V} \\ 0 & 0 & 0 & \cdots & \mathbf{V}^\dagger & \mathbf{U}'_N \end{pmatrix}. \tag{10}$$

As discussed below, the diagonal term for the final layer, $\mathbf{U}'_N$, depends on the boundary conditions imposed on the bottom of the substrate. The term $\mathbf{U}'_0$ differs from $\mathbf{U}'$ because the diagonal elements of $\mathbf{D}_{i\alpha i\alpha}$ include terms from nearest neighbors in all layers. This can easily be seen by considering the case of a pair potential coupling two atoms, $\phi(\vec{r}_i - \vec{r}_j)$. The second derivative of this part of the total energy will contain terms diagonal in $i$. Since the top layer has fewer neighbors included in the harmonic approximation, the diagonal terms will be reduced. Specific examples are provided in Appendix A.

The displacements throughout the substrate are linear functions of the forces applied to the boundary layer:

$$\vec{u}_\beta(\vec{q},\omega) = \mathbf{G}_{\beta 0}\vec{f}_{\rm tot}(\vec{q},\omega). \tag{11}$$

Here the Green's function $\mathbf{G}$ satisfies the equation

$$\sum_\beta(-\mathbf{m}\omega^2\delta_{\alpha\beta} + \mathbf{D}_{\alpha\beta}(\vec{q}))\mathbf{G}_{\beta\gamma}(\vec{q},\omega) = \delta_{\alpha\gamma}\mathbf{I}, \tag{12}$$

where $\mathbf{I}$ is a $3n_c \times 3n_c$ identity matrix.

We only need to calculate $\mathbf{G}_{00}$, since $E_{\rm eb}$ only involves displacements of the boundary layer. It is convenient to express everything in terms of these displacements, which can then be used to calculate the forces from explicit atoms as well as the substrate force. Defining the surface stiffness matrix $\mathbf{\Phi} = \mathbf{G}^{-1}_{00}$ we have

$$\vec{f}_{\rm tot}(\vec{q},\omega) = \mathbf{\Phi}(\vec{q},\omega)\vec{u}_0(\vec{q},\omega). \tag{13}$$

Equation (13) resembles Hooke's law, and the coefficients $\mathbf{\Phi}$ can be regarded as renormalized spring constants that govern

the response of the elastic half space.[25] Note that even though the atomistic interaction within the bulk may be short ranged, the real space coefficients $\mathbf{\Phi}$ typically couple the surface over all length scales.

One can evaluate the Green's function using a transfer matrix formulation. This approach has been previously applied to the analysis of the electronic[36] and phononic[37] structure of surfaces and, more generally, to the statistical mechanics of systems with only short-ranged interactions, like the Ising model.[42–44] Our derivation is most similar in form to that of Velasco and Ynduráin.[37] Unlike the force-constant matrix, the Green's function is not sparse. We denote the individual elements by

$$\mathbf{G} = \begin{pmatrix} \mathbf{G}_{00} & \mathbf{G}_{01} & \mathbf{G}_{02} & \cdots & \mathbf{G}_{0N} \\ \mathbf{G}_{10} & \mathbf{G}_{11} & \mathbf{G}_{12} & \cdots & \mathbf{G}_{1N} \\ \mathbf{G}_{20} & \mathbf{G}_{21} & \mathbf{G}_{22} & \cdots & \mathbf{G}_{2N} \\ \vdots & \vdots & \vdots & \ddots & \vdots \\ \mathbf{G}_{N0} & \mathbf{G}_{N1} & \mathbf{G}_{N2} & \cdots & \mathbf{G}_{NN} \end{pmatrix}, \tag{14}$$

where we will drop the explicit reference to $\vec{q}$ and $\omega$ below.

From Eq. (12) we obtain generally $(N+1)^2$ equations for our finite system with $N+1$ layers. We only pick the $N+1$ equations involving the surface layer. These are

$$\mathbf{U}_0\mathbf{G}_{00} + \mathbf{V}\mathbf{G}_{10} = \mathbf{I} \tag{15}$$

$$\mathbf{V}^\dagger\mathbf{G}_{00} + \mathbf{U}\mathbf{G}_{10} + \mathbf{V}\mathbf{G}_{20} = \mathbf{0}$$

$$\mathbf{V}^\dagger\mathbf{G}_{10} + \mathbf{U}\mathbf{G}_{20} + \mathbf{V}\mathbf{G}_{30} = \mathbf{0}$$

$$\vdots$$

$$\mathbf{V}^\dagger\mathbf{G}_{n-1,0} + \mathbf{U}\mathbf{G}_{n,0} + \mathbf{V}\mathbf{G}_{n+1,0} = \mathbf{0} \tag{16}$$

$$\vdots$$

$$\mathbf{V}^\dagger\mathbf{G}_{N-1,0} + \mathbf{U}_N\mathbf{G}_{N,0} = \mathbf{0}, \tag{17}$$

where $\mathbf{U} = \mathbf{U}' - \mathbf{m}\omega^2$. It is also straightforward to include wave-vector-dependent damping by adding a term of the form $i\omega\Gamma(\vec{q})$ in addition to the mass term.

Given the structure of these equations it is useful to define the transfer matrix $\mathbf{T}_n$ as

$$\mathbf{G}_{n+1,0} = \mathbf{T}_n\mathbf{G}_{n,0}. \tag{18}$$

The surface Green's function $\mathbf{G}_{00}$ and stiffness $\mathbf{\Phi}$ are then obtained from Eq. (15) as

$$\mathbf{\Phi} = \mathbf{G}_{00}^{-1} = \mathbf{U}_0 + \mathbf{V}\mathbf{T}_0. \tag{19}$$

Combining Eqs. (16), (17), and (18) yields

$$\mathbf{V}\mathbf{T}_n\mathbf{T}_{n-1} + \mathbf{U}\mathbf{T}_{n-1} + \mathbf{V}^\dagger = 0 \tag{20}$$

and

$$\mathbf{U}_N\mathbf{T}_{N-1} + \mathbf{V}^\dagger = 0. \tag{21}$$

For physically relevant solutions the displacements produced by static surface forces (i.e., at $\omega = 0$) must decrease or remain constant with increasing depth. This implies that the eigenvalues of $\mathbf{T}_n$ have magnitude between 0 and 1. If the eigenvalues are less than 1, the deformation decays exponentially with distance from the surface and the result is insensitive to the depth of the system. The analytic solution to the continuum Green's function for a semi-infinite plane[45] gives an exponential decay with length of order $1/|\vec{q}|$ and we find that the lattice Green's function is consistent with this scaling for small $|\vec{q}|d_{\mathrm{nn}}$, where $d_{\mathrm{nn}}$ is the nearest-neighbor spacing. As a result, the surface stiffness matrix is sensitive to boundary conditions for small wave vectors: $|\vec{q}| \sim 1/Nd_{\mathrm{nn}}$.

One interesting case is that of free boundary conditions. In this case, one allowed solution is uniform translation of the entire system, i.e., $\mathbf{T} = \mathbf{I}$ for $\vec{q} = 0$. Translational invariance requires that no force is produced by a uniform translation of the crystal and this imposes an acoustic sum rule on the components of $\mathbf{D}$.[17,40] It is straightforward to show that Eq. (20) is consistent with this sum rule for $\mathbf{T}_n = \mathbf{I}$. The surface stiffness matrix for uniform translation of all atoms vanishes for this case because from Eq. (19) we get $\mathbf{\Phi}(\mathbf{\Gamma}) = \mathbf{U}_0(\mathbf{\Gamma}) + \mathbf{V}(\mathbf{\Gamma})$, which is precisely the acoustic sum rule at the surface.

To maintain a finite stiffness, one normally considers systems with a rigid boundary condition applied at the bottom of the substrate. This corresponds to $\mathbf{U}_N = \mathbf{U}$. In essence, this equality implies that there is a contribution from neighbors below layer $N$ but that their displacement is set to zero. The acoustic sum rule is violated because these neighbors impose a frame of reference. For the rigid boundary condition we expect a constant, uniform force will produce a constant uniform strain. Then $\mathbf{T}_0 \approx \mathbf{I}(1 - 1/N)$ and the surface stiffness $\mathbf{\Phi}(\mathbf{\Gamma})$ is finite but goes to zero as $1/N$ with increasing system depth $N$.

The fact that the termination at layer $N$ is important for small $\vec{q}$ means that we cannot, in general, assume that $\mathbf{T}_n$ is independent of $n$. We solve the equations using a continued fraction approach based on the relation

$$\mathbf{V}\mathbf{T}_{n-1} = -\mathbf{V}(\mathbf{U} + \mathbf{V}\mathbf{T}_n)^{-1}\mathbf{V}^\dagger. \tag{22}$$

The continued fraction has the form

$$\mathbf{\Phi} = \mathbf{U}_0 - \mathbf{V}\cfrac{1}{\mathbf{U} - \mathbf{V}\cfrac{1}{\mathbf{U} - \mathbf{V}\cfrac{1}{\mathbf{U} - \mathbf{V}\cfrac{1}{\mathbf{U} - \ldots}\mathbf{V}^\dagger}\mathbf{V}^\dagger}\mathbf{V}^\dagger}\mathbf{V}^\dagger \tag{23}$$

For large $q$, the bottom boundary is unimportant and the continued fraction converges after a few iterations. For small $q$, the continued fraction is terminated after $N$ terms using Eq. (21). In the examples below we focus on static solutions $\omega = 0$. For dynamic solutions a small imaginary part is added to the frequency to obtain the retarded Green's function.[46]

The above method of finding $\mathbf{\Phi}$ is of order $N$ for small $q$. Since the Green's function can be precomputed, this does not represent a significant computational barrier. However, there is an alternative approach based on decimation that is only of order $\log N$. Related approaches have been used for real-space renormalization calculations of electronic structure.[38,39]

Equations (15) to (17) only couple nearest-neighbor elements of $\mathbf{G}$. The equations for odd $n$ can be used to express

$\mathbf{G}_{2n+1,0}$ in terms of $\mathbf{G}_{2n+2,0}$ and $\mathbf{G}_{2n,0}$. Substituting the result into the equations for even $n$, one obtains equations of the same form as Eqs. (15) to (17) but with renormalized $\mathbf{U}^{(2)}$ and $\mathbf{V}^{(2)}$,

$$\mathbf{U}_0^{(2)}\mathbf{G}_{00} + \mathbf{V}^{(2)}\mathbf{G}_{20} = \mathbf{I}, \quad (24)$$

$$(\mathbf{V}^{(2)})^\dagger\mathbf{G}_{2n-2,0} + \mathbf{U}^{(2)}\mathbf{G}_{2n,0} + \mathbf{V}^{(2)}\mathbf{G}_{2n+2,0} = \mathbf{0}, \quad (25)$$

$$(\mathbf{V}^{(2)})^\dagger\mathbf{G}_{N-2,0} + \mathbf{U}_N^{(2)}\mathbf{G}_{N,0} = \mathbf{0}. \quad (26)$$

The procedure can then be repeated with the renormalized equations. The general recursion expressions for the renormalized matrices at iteration $m$ are

$$\mathbf{U}^{(m+1)} = \mathbf{U}^{(m)} - (\mathbf{V}^\dagger\mathbf{U}^{-1}\mathbf{V})^{(m)} - (\mathbf{V}\mathbf{U}^{-1}\mathbf{V}^\dagger)^{(m)}, \quad (27)$$

$$\mathbf{V}^{(m+1)} = -(\mathbf{V}\mathbf{U}^{-1}\mathbf{V})^{(m)}, \quad (28)$$

$$\mathbf{U}_0^{(m+1)} = \mathbf{U}_0^{(m)} - (\mathbf{V}\mathbf{U}^{-1}\mathbf{V}^\dagger)^{(m)}, \quad (29)$$

$$\mathbf{U}_N^{(m+1)} = \mathbf{U}_N^{(m)} - (\mathbf{V}^\dagger\mathbf{U}^{-1}\mathbf{V})^{(m)}. \quad (30)$$

The greatest efficiency is achieved when $N = 2^M$. The equations are then iterated $M$ times to produce two linear equations containing only $\mathbf{G}_{00}$ and $\mathbf{G}_{N0}$,

$$\mathbf{U}_0^{(M)}\mathbf{G}_{00} + \mathbf{V}^{(M)}\mathbf{G}_{N0} = \mathbf{I}, \quad (31)$$

$$(\mathbf{V}^{(M)})^\dagger\mathbf{G}_{00} + \mathbf{U}_N^{(M)}\mathbf{G}_{N0} = \mathbf{0}. \quad (32)$$

This yields

$$\mathbf{\Phi} = \mathbf{U}_0^{(M)} - \mathbf{V}^{(M)}\left(\mathbf{U}_N^{(M)}\right)^{-1}(\mathbf{V}^{(M)})^\dagger. \quad (33)$$

For large wave vectors, the renormalized $\mathbf{V}^{(m)}$ goes rapidly to zero as $m$ increases and $\mathbf{U}_0^{(m)}$ goes to a constant.[38] The surface stiffness matrix $\mathbf{\Phi}$ is equal to the renormalized $\mathbf{U}_0^{(m)}$. We numerically checked that transfer matrix and renormalization group calculations give identical results.

## III. APPLICATION TO STATIC CONTACT MECHANICS

To show that the Green's function method provides seamless boundary conditions we present results for three cases. The first is surface relaxation at a flat crystal/vacuum interface, where the unbalanced forces $\vec{f}_{i0}$ are important. The second is Hertzian contact of a rigid sphere and a flat elastic substrate. In the final example, the sphere is replaced by a randomly rough surface, which enhances plastic deformation in the crystal.

Results for different crystals and interactions are presented. The simplest is the (100) surface of a face-centered cubic (fcc) crystal with nearest-neighbor harmonic interactions with spring constant $k$. This system is called nn-fcc below.

The second system, called 2n-fcc, is also the (100) fcc surface but with second-nearest-neighbor interactions. Particles interact with a Lennard-Jones potential

$$V(r) = 4\epsilon\left[\left(\frac{\sigma}{r}\right)^{12} - \left(\frac{\sigma}{r}\right)^{6}\right] \quad (34)$$

for $r < r_1 = 1.35\sigma$. The potential and force are then smoothly brought to zero at $r_2 = 1.8\sigma$ using a third-order spline.[47] The value of $r_2$ is chosen so the potential extends only to second-nearest neighbors in the zero pressure ground state of the fcc structure.

The third case, called sc, is the (100) surface of a simple cubic solid with the same spring constant $k$ between first and second neighbors. This solid has also been used by Campaña and Müser in their work on the contact of rough surfaces.[25,27–29] We checked that the transfer matrix and renormalization formulations give surface stiffness matrix coefficients that are identical to the analytic result of Saito[30] for the sc system.

The final system uses the Green's function from continuum theory for an isotropic medium. Here the surface stiffness matrix is approximately linear in $\vec{q}$ for all wave vectors. The full continuum expression is given in Appendix B. Explicit expressions for the force-constant matrices of the other models are given in Appendix A.

As a first example, we consider surface relaxation at a flat crystal/vacuum interface. Terminating the crystal generally leads to nonzero internal forces on atoms that lie on the ideal lattice sites. These are described by $\vec{f}_{i0}$ in our Green's function method. One consequence is that the spacing between atomic planes deviates from the bulk value and varies as a function of the depth below the interface. For a flat surface, the forces are the same on all unit cells so we only need to consider the $\vec{q} = 0$ contribution.

Figure 2 shows the deviation from the bulk spacing between atomic planes as a function of depth for the 2n-fcc system. Results for zero, two, four, and eight atomic planes of explicit atoms on top of the boundary layer are all equivalent. (Note that there are two atomic planes per boundary and substrate layer.) This confirms that the Green's function provides a seamless boundary condition for the explicit region. Note that in some systems surface relaxation leads to a different periodicity of the surface and bulk layers. To capture this relaxation, one must

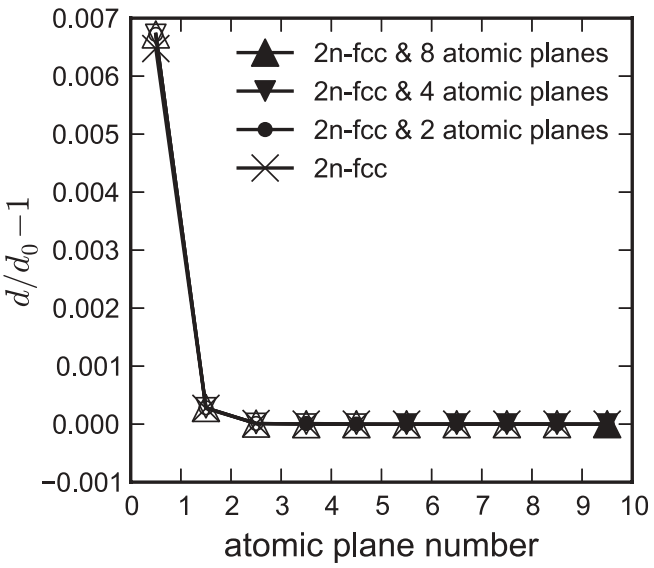


FIG. 2. Fractional change in spacing of atomic planes $d$ from bulk value $d_0$ as a function of depth below a free (100) surface of an fcc crystal. Results from the Green's function with zero, two, four, and eight atomic planes (zero, one, two, and four unit cells) are equivalent. The surface atomic plane is 0 and the separation is plotted at the midpoint between planes. Open symbols show the spacing within the explicit crystal and between explicit and substrate planes. Full symbols denote spacing within the substrate.

include layers of explicit atoms above the Green's function boundary layer.

The previous Green's function implementation of Campañá *et al.*[25] did not include $\vec{f}_{i0}$ and, thus, did not capture surface relaxation. We found that excluding $\vec{f}_{i0}$ had several effects. One was that it led to nonuniform spacing between atomic planes of explicit atoms placed on top of the boundary layer. This variation is effectively a form of surface relaxation due to an effective discontinuity in the forces between surfaces. It also represents a violation of Newton's third law because boundary atoms feel a force from explicit atoms, but the counterforce is missing. When the explicit atoms were from an opposing surface, we found that the change in spacing of atomic planes led to changes in the force on the second layer that could be important for adhesive contact.

Our second example is Hertzian contact[45] of a rigid spherical indenter with radius $R$ and an elastic substrate with contact modulus $E^*$. Continuum theory[45,48] predicts contact occurs in a circle of contact radius $a$. Both $a$ and the peak pressure $p_0$ in the center of the contact rise as the cube root of the normal load $N$,

$$\frac{a}{R} = \frac{\pi}{2}\frac{p_0}{E^*} = \left(\frac{3N}{4E^*R^2}\right)^{1/3}. \tag{35}$$

These analytic predictions are compared to different atomistic models in Fig. 3.

All atomistic models have substrates with a square array of $256 \times 256$ surface atoms and a depth of 256 atomic planes. Different numbers of atomic planes are treated explicitly and the number of atomic planes in the boundary and substrate layers depends on the interaction range. Here and in all following simulations we move the indenter and then relax the positions of the substrate atoms assuming a rigid boundary at the bottom of the substrate. The sphere is featureless and interacts with an atom at position $\vec{r}_i$ via the potential $V_{\text{rigid}}(\vec{r}_i) = V(|\vec{r}_i - \vec{r}_0| - R)$, where $\vec{r}_0$ is the center of the sphere and $R$ its radius. The potential $V$ is the Lennard-Jones potential of Eq. (34) but cut off at its minimum and with $\epsilon$ increased by a factor of 100 to approximate a hard-sphere interaction.

The contact modulus $E^*$ is analytically known for the isotropic continuum case, where $E^* = 2\mu(1+\nu)/(1-\nu^2)$, $\mu$ is the shear modulus, and $\nu$ Poisson's ratio (see Appendix B). In the results below $\nu = 0$. The 2n-sc substrate is isotropic with $E^* = \frac{8}{3}k/A_a$, where $A_a$ is the surface area occupied by a single atom. The nn-fcc and 2n-fcc cases are anisotropic, and in this case the contact modulus generally depends on orientation and indenter geometry.[49,50] There is no simple analytic relation and we will use Hertz theory to fit effective values of $E^*$.

Figure 3(a) shows the variation of $p_0$ with load for all atomistic systems. First, we discuss results where the entire substrate is treated with the Green's function method so the elastic response is linear. Data for each system were divided by the value of $E^*$ that optimizes the fit to the solid line showing the prediction of continuum theory. For the cases where $E^*$ is known, the fit value is within about 2% of the analytical expression. Some deviation is expected from the discrete geometry and the finite compliance of the interface potential. For the continuum Green's function the fit yields $E^* = 2.02\mu$ compared to the analytic $E^* = 2\mu$. For the 2n-sc solid we obtain $E^* = 2.73k/A_a$ as compared to the analytic $E^* \approx 2.67k/A_a$. For the nn-fcc and 2n-fcc substrate, the fits give $E^* = 1.4k/A_a$ and $E^* = 70.4\epsilon/\sigma^3$, respectively. While we have no prediction to compare to, these numbers are of the order of the relevant elastic moduli.

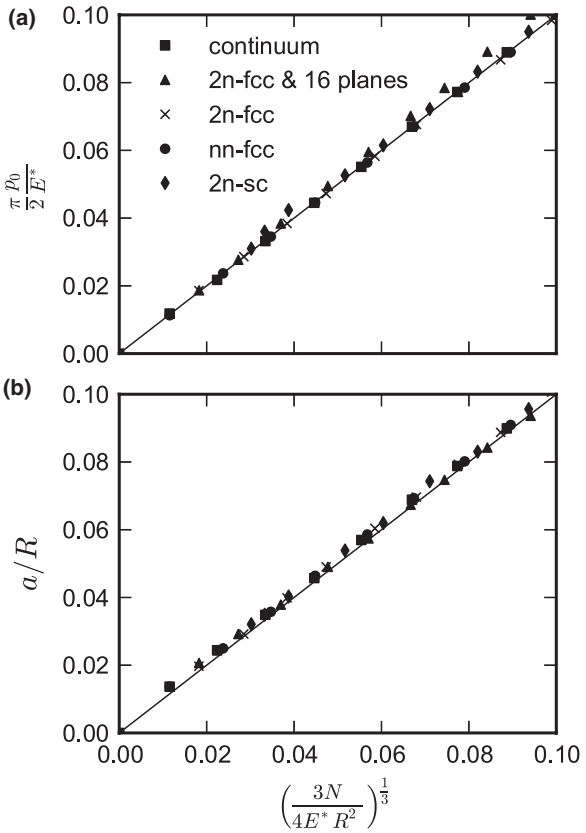


FIG. 3. Contact of a rigid spherical indenter with radius $R = 100\sigma$ on an elastic substrate. Shown is (a) the peak pressure $p_0$ and (b) contact radius $a$ as a function of load $N$ normalized by the elastic contact modulus $E^*$. We compare calculations for (100) surfaces of the fcc lattice with nearest-neighbor (nn) and second-nearest-neighbor (2n) interactions to calculations of a simple cubic (100) surface and continuum calculations. The effective size of the substrate is a cubic block with 256 atoms in each lateral direction and periodicity parallel to the surface. The values for the effective contact modulus $E^*$ for the anisotropic nn-fcc and 2n-fcc cases are fit to the peak pressure shown in panel (a).

Figure 3(b) compares the load-radius relationship for different models to continuum theory using the value of $E^*$ obtained from fitting $p_0$ above. Contact was defined by a repulsive interaction between atoms and indenter. The contact radius was then obtained by equating $\pi a^2$ to the number of contacting atoms times the surface area per atom. While $a/R$ rises linearly with the slope predicted by continuum theory, there is an offset corresponding to an increase in contact area. An even larger offset is observed in previous simulations of atomic scale contact.[1,51–53] The deviations are minimized in our work by using a featureless indenter and making the interaction closer to a hard wall repulsion by increasing $\epsilon$ by two orders of magnitude. The same limit was achieved in Ref. 53 by increasing the density of atoms on the indenter.

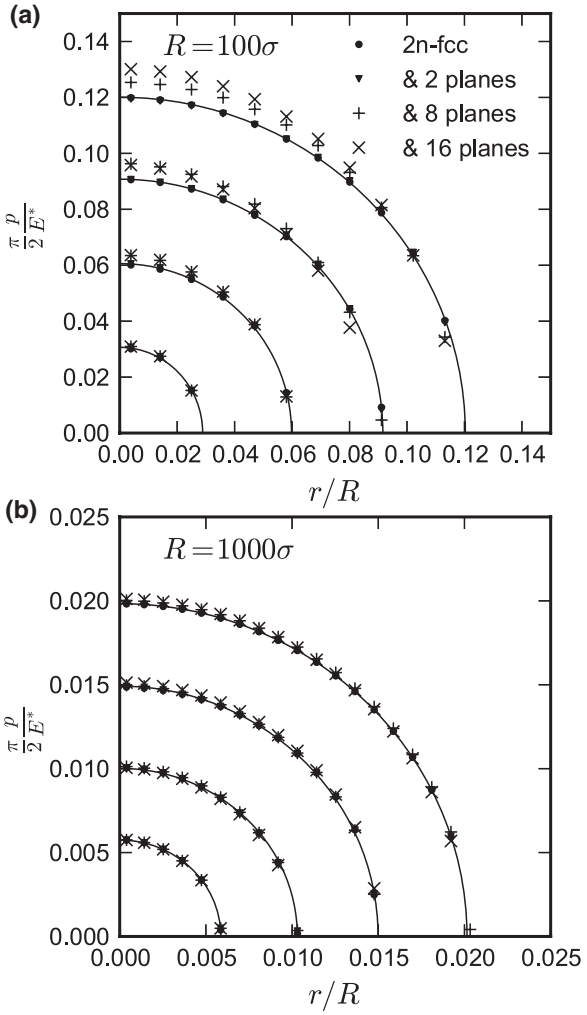


FIG. 4. Pressure as a function of distance from the tip center along a row of atoms in the (110) direction for rigid spherical indenters with radius (a) $R = 100\sigma$ or (b) $R = 1000\sigma$ on an elastic substrate.

The peak strain at the interface is of order $a/R$ and one may expect nonlinear behavior at the largest values of ∼10% in Fig. 3. The Green's function approach allows this to be studied while treating only a small number of explicit atoms. Figure 3 shows that including 16 layers of explicit atoms does not change the contact area on the scale of the figure but does increase the peak pressure. The full pressure distribution for different numbers of atomic planes at several loads is shown in Fig. 4 for $R = 100\sigma$ and $R = 1000\sigma$. In all cases, the Green's function results follow the analytic solution for elastic substrates (solid line). When explicit atomic planes are included, there are deviations from Hertz theory. The pressure needed to deform the central regions is higher for the explicit solution because Lennard-Jones bonds become stiffer as they are compressed. As expected from Hertz theory, the deviations increase with $a/R$ which sets the peak strain. Increasing $R$ from $100a$ to $1000a$ reduces the deviations at a fixed value of $a$. Deviations are very small for $a/R$ less than 2%, which is consistent with direct evaluations of anharmonic effects.

Note that the number of atomic planes needed to capture nonlinear effects grows with $a/R$. A single pair of planes has little effect, while 8 planes is sufficient for $a/R$ up to about 0.09 [Fig. 4(a)]. All atom simulations are consistent with the 16-plane results for $a/R = 0.12$ and one may expect plastic deformation at larger $a/R$ for most materials. In the Hertz solution, strains decay over scales of order $a$ and the peak shear strain is at a depth of about $a/3$.[45] Including explicit atoms to greater depths should allow the system to capture nucleation of defects and other nonlinear effects.

The next test considers the case of contact with a rigid, randomly rough surface, which has been extensively investigated using similar techniques.[3,4,25,27–29] Many experimental surfaces are found to have roughness on all scales that can be described as a self-affine fractal. The root-mean-squared (rms) change in height $dh$ over a lateral distance $\ell$ scales as $dh \propto \ell^H$ where $H$ is called the Hurst or roughness exponent. We generate a self-affine surface with $H = 0.8$ on a $1024 \times 1024$ grid using Voss' random midpoint algorithm.[54] This surface is Fourier filtered to remove roughness on all wavelengths below 16 grid spacings. We then use bicubic splines to interpolate the discrete positions to a continuous surface with height $h(x,y)$. The final surface has a rms slope of $h_0' = \sqrt{|\nabla h|^2} = 0.09$.

The rough surface is pushed against a 2n-fcc solid with $256 \times 256$ surface atoms and different numbers of explicit layers. Atoms at position $\vec{r} = (x,y,z)$ interact with the surface via the potential $V_{\text{rigid}}(x,y,z) = V[z - h(x,y)]$, where $V(z)$ has the same functional form as the interaction used for the rigid sphere but depends only on the height difference. The area of contact $A$ is determined by multiplying the area per atom by the number of atoms in the top layer of the crystal that feel a repulsion from the rough surface.

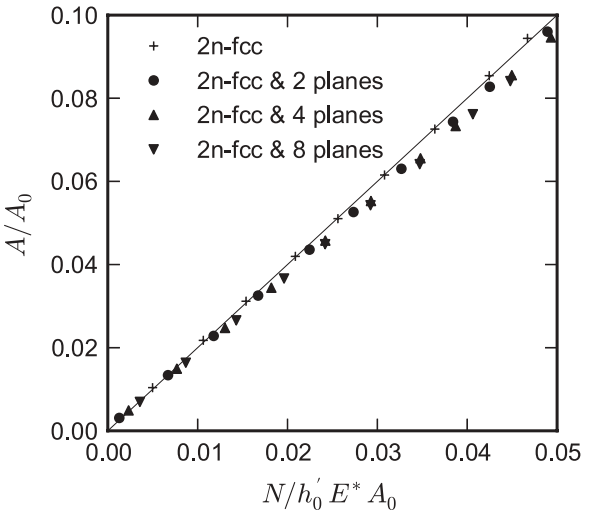


FIG. 5. Contact of a rigid rough surface on a crystalline fcc (100) surface. The periodicity of the rough surface is 256 nearest-neighbor distances $d_0$ in both directions with a nominal surface area of $A_0 = 256d_0 \times 256d_0$. The solid interacts via a pair potential that extends to second neighbors as described in the text. The area $A$ is shown as a function of the load $N$ normalized by the rms slope $h_0' = \sqrt{|\nabla h|^2}$ of the rough surface and the contact modulus $E^*$. The substrate is a block with 256 atoms in each direction. We compare the results of a simulation with only a harmonic half space to systems with two, four and eight explicit atomic planes on top of the half space. The anharmonicity of the explicit interatomic interactions leads to a stiffening and a slightly smaller contact area at larger loads. The solid line has slope $1/\kappa = 1/2$.

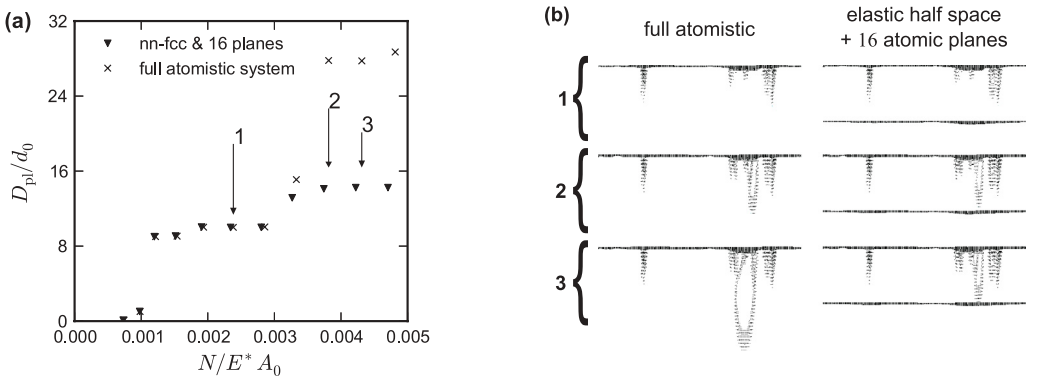


FIG. 6. (a) Load dependence of the depth $D_{pl}$ of the deepest plastically deformed atom divided by the spacing $d_0$ of atomic planes as determined from a common neighbor analysis (CNA). The Green's function results with 16 atomic planes of explicit atoms follow the all atom calculation until plasticity reaches the Green's function layer. (b) Snapshots showing the projections of the atoms that have displaced plastically as determined from a CNA. The CNA shows dislocation loops are emitted from the surface. Snapshots shown by 1, 2, and 3 correspond to the loads marked 1, 2, and 3 in panel (a) and are recorded at 8%, 15%, and 16% contact area, respectively. Dislocations in the full atomistic and reduced system behave identically until the deepest dislocation loop hits the elastic boundary where it cannot propagate.

Previous numerical and analytic work has found a linear relationship between load and contact area of the form

$$\frac{N}{h_0' E^* A_0} = \frac{1}{\kappa}\frac{A}{A_0} \tag{36}$$

with $\kappa \approx 2$.[29,55,56] Figure 5 compares this prediction (solid line) to results for 2n-fcc surfaces with different numbers of layers of explicit atoms. At small loads, results for all numbers of explicit atoms lie close to the solid line. The purely elastic calculation, where the entire elastic solid is described by the Green's function, follows the solid line all the way to 10% contact area. When two explicit atomic planes are included, the area rises less rapidly as the load increases. This reflects anharmonicity in the explicit planes, where the Lennard-Jones potential stiffens as bond lengths shrink under the applied pressure. Note that results with four and eight explicit planes are nearly indistinguishable, implying that anharmonicity is largely confined to the outer layers. A small number of explicit planes is sufficient in this case because the effective radius $a$ of local contacting regions for this rough surface is only of order $4\sigma$. This allows the Green's function method to reproduce the full nonlinear response of the atomistic system at a small fraction of the computational cost.

The rough surface just considered is artificial because it has no atomic structure. As a final example, we consider a rough rigid surface made of discrete atoms on a crystalline lattice. The layered structure leads to steps or terraces that focus stress and lead to dislocation nucleation.

The stepped surface is created from an fcc crystal with a (100) surface and the same lattice spacing as the substrate. A smooth randomly rough surface with rms slope $h_0' = 0.03$ and $H = 0.5$ was created using the procedure described above. Then all atoms of the lattice with heights below the surface were removed. The elastic substrate is like the nn-fcc case described above. However, since ideal springs would not allow plasticity, neighbors interact with a Lennard-Jones potential that is splined to zero force between $1.2\sigma$ and $1.25\sigma$. All systems had $256 \times 256$ surface atoms and 256 atomic planes. Two atomic planes make up a unit cell and the spacing of atomic planes $d_0$ is the nearest-neighbor spacing $d_{nn}$ divided by $\sqrt{2}$. To identify plastic deformation, we detect atoms whose environment deviates from the crystal using common neighbor analysis (CNA).[57,58]

Figure 6(a) plots the depth of the deepest plastic atom $D_{pl}$ normalized by the spacing of atomic planes $d_0$. Fully atomistic calculations of the entire volume are used as a benchmark. They are compared to calculations where the top 16 atomic planes (8 substrate layers) are treated explicitly and the remaining atoms are replaced by the Green's function. Note that the Green's function and all atom calculations give nearly identical results until plasticity reaches the depth of the boundary layer. Dislocations cannot propagate in to the boundary layer, but their motion is not affected by the boundary layer when there are a couple of explicit layers separating them. Arrest of dislocations at the boundary is unavoidable in most continuum/atomistic coupling schemes,[59] with a notable exception of the coupled atomistic and discrete dislocation method.[60]

Projections showing the geometry of the dislocations generated in the full and 16 layer calculations are compared in Fig. 6(b). The structure is fully captured for the load corresponding to point 1 in Fig. 6(b). At point 2, the deepest plastic atom has nearly reached the boundary layer. The largest dislocation loop is slightly suppressed in the 16 layer system, but the remaining dislocations are not affected. At point 3, the dislocations have clearly penetrated past the boundary layer and this cannot be captured by the Green's function. Note that this load is comparable to the highest load in Fig. 5 and the contact area is close to 16%. We have found that global measures, such as plots of contact area vs. load, are much less sensitive to the number of explicit layers than the dislocation depth.

## IV. CONCLUSIONS

An approach for coupling an explicit atomistic region to a substrate described with a Green's function was developed and tested. The entire system is described by a single Hamiltonian and the only approximation is to neglect anharmonic terms in the substrate. Many other atomistic/coupling schemes

introduce ghost forces or cannot be described by a single Hamiltonian.[9,12] Previous applications of the Green's function approach have also neglected some forces near the elastic/explicit boundary leading to violations of Newton's third law and ghost forces when interactions extend beyond nearest layers.

Efficient methods for calculating the Green's function given the interatomic potential were described. Fourier transforming in the plane of the substrate reduces the problem to a one-dimensional coupling between $N$ layers for each in-plane wave vector $\vec{q}$. These equations can be solved using a transfer matrix approach[36,37] or a renormalization group method[38,39] with computational effort that scales as $1/|\vec{q}|$ or $-\ln|\vec{q}|$, respectively. This is order $N^2$ faster than a previous fluctuation-dissipation formulation for obtaining the Green's function.[25] While we have exclusively presented calculations using pair potentials, an extension to many-body formulations such as embedded-atom[61] or bond-order[62] potentials is straightforward. Similarly, we consider only static applications but present equations for the full dynamic problem with arbitrary masses and damping.

Three tests of the method were discussed. The first is surface relaxation, which reflects the loss of neighbors at a free surface. The Green's function approach accurately reproduced explicit atomistic simulations. The previous Green's function implementation[25] was only accurate for nearest-neighbor interactions at zero pressure where relaxation vanishes. The second test was Hertzian contact by a rigid sphere. With no explicit atoms, the elastic Green's function reproduced the analytic response for an elastic continuum. Adding only 8 to 16 atomic planes of explicit atoms allowed anharmonic corrections to Hertz theory to be captured with a relatively modest increase in computer time. The final example was contact with a randomly rough surface with atomic steps that nucleated subsurface dislocations. The Green's function method captured the full response, including contact area and dislocation distribution, until the dislocations came very close to the elastic layer.

There are several ways in which the current approach can be extended. Periodic changes in elemental composition of the crystal as encountered in nanolaminates can be included straightforwardly by allowing the force-constant matrix to vary with depth. Another extension is to evaluate both the full force and the harmonic approximation for atoms at the elastic/explicit interface. The deviation can be used to estimate errors and determine whether to terminate the calculation or add additional layers of explicit atoms. This addition could be done adaptively on the fly. A third is to include finite temperature. The static elastic response can still be described by a Green's function that must be modified if the temperature is high enough to produce anharmonic effects. The success of recent extensions of the quasicontinuum method[63,64] suggests that the most important changes in the Green's function can be captured by using the thermally expanded lattice to determine the force-constant matrix.

## ACKNOWLEDGMENTS

We are grateful for discussions with Martin Müser. This material is based upon work supported by the Air Force Office of Scientific Research under Grant No. FA9550-0910232, the U.S. National Science Foundation under Grants No. IGERT-0801471 and No. PHY11-25915, and the European Commission under Marie-Curie IOF-272619. Computations were carried out at the Jülich Supercomputing Center, and the Johns Hopkins Homewood High Performance Cluster and Graphics Processor Laboratory which were partially supported by U.S. National Science Foundation Grants No. OCI-0963185 and CMMI-0923018.

## APPENDIX A: FORCE-CONSTANT MATRICES FOR (100) SURFACES AND PAIR INTERACTIONS

The force-constant matrices are readily derived for any potential, but we focus on pair potentials $V(r)$ that depend only on the separation $r$ between each pair of particles. The potential energy of the boundary and substrate then becomes

$$E_{\rm bs} = \sum_{ij,i<j} V(r_{ij}) = \frac{1}{2}\sum_{ij} V(r_{ij}), \tag{A1}$$

where the sum is over all atomic sites $i$ and $j$ that lie in the boundary or substrate layers (Fig. 1).

To simplify the notation we will first calculate the force-constant matrix for the case of a single atom per unit cell, $n_c = 1$, and thus nearest-neighbor interactions. We denote the atomic positions by $\vec{r}_i$ and $\vec{r}_{ij} = \vec{r}_i - \vec{r}_j$ is the vector between atoms $i$ and $j$. The force-constant matrix is defined in terms of derivatives of the energy relative to the displacement $\vec{u}_i \equiv \vec{r}_i - \vec{r}_i^{\,0}$ from equilibrium positions $\vec{r}_i^{\,0}$. It is useful to separate the components along and perpendicular to the unit vector $\vec{e}_{ij}^{\,0} = \vec{r}_{ij}^{\,0}/|\vec{r}_{ij}^{\,0}|$ in the direction between equilibrium positions of $i$ and $j$,

$$\mathbf{D}_{ij} = \mathbf{D}_{ij}^{\parallel} + \mathbf{D}_{ij}^{\perp}. \tag{A2}$$

The parallel component is

$$\begin{aligned}\mathbf{D}_{ij}^{\parallel} &= \frac{1}{2}\sum_{kl}\frac{\partial^2 V}{\partial r_{kl}^2}\frac{\partial r_{kl}}{\partial \vec{u}_i}\otimes\frac{\partial r_{kl}}{\partial \vec{u}_j}\bigg|_{\vec{u}_i=0,\vec{u}_j=0}\\ &= -k_{ij}\vec{e}_{ij}^{\,0}\otimes\vec{e}_{ij}^{\,0} + \delta_{ij}\sum_{n\in\text{neighb.}} k_{in}\vec{e}_{in}^{\,0}\otimes\vec{e}_{in}^{\,0},\end{aligned} \tag{A3}$$

where $\otimes$ denotes the outer product and

$$k_{ij} = \frac{\partial^2 V}{\partial r_{ij}^2}\bigg|_{r_{ij}^0} \tag{A4}$$

is the effective spring constant in the equilibrium structure. The perpendicular component is

$$\begin{aligned}\mathbf{D}_{ij}^{\perp} &= \frac{1}{2}\sum_{kl}\frac{\partial V}{\partial r_{kl}}\frac{\partial^2 r_{kl}}{\partial \vec{u}_i\partial \vec{u}_j}\bigg|_{\vec{u}_i=0,\vec{u}_j=0}\\ &= \frac{f_{ij}}{r_{ij}^0}\left(\mathbf{I}-\vec{e}_{ij}^{\,0}\otimes\vec{e}_{ij}^{\,0}\right)\\ &\quad -\delta_{ij}\sum_{n\in\text{neighb.}}\frac{f_{in}}{r_{in}^0}\left(\mathbf{I}-\vec{e}_{in}^{\,0}\otimes\vec{e}_{in}^{\,0}\right),\end{aligned} \tag{A5}$$

where

$$f_{ij} = -\frac{\partial V}{\partial r_{ij}}\bigg|_{r_{ij}^0} \tag{A6}$$

is the absolute force at the equilibrium separation $r_{ij}^0$. Note that $\mathbf{D}_{ij}^{\perp}$ vanishes for crystals at zero pressure that interact via nearest neighbors only since, in this case, $f_{ij} = 0$ in the above equations. Even for interatomic potentials that act over a larger range, this contribution is typically an order of magnitude smaller than $\mathbf{D}_{ij}^{\parallel}$ and, indeed, often ignored in discussions of phononic excitations.[40] We explicitly checked the influence of $\mathbf{D}_{ij}^{\perp}$ for the contact situations discussed in Sec. III and found no visible change on the scale of the plots. Yet, for the sake of completeness, we retain $\mathbf{D}_{ij}^{\perp}$ in the following derivations and denote the force-constant for bond rotation by $k^{\perp} = -f/r^0$.

The following sections consider different crystal systems. In all cases, the free surface of the elastic half-space is oriented perpendicular to the $z$ direction. To simplify expressions involving phase factors, we use the abbreviations $c_x = \cos q_x d_{\mathrm{nn}}$, $s_x = \sin q_x d_{\mathrm{nn}}$, $c_{\frac{x}{2}} = \cos \frac{q_x d_{\mathrm{nn}}}{2}$, and $s_{\frac{x}{2}} = \sin \frac{q_x d_{\mathrm{nn}}}{2}$.

#### *1. sc* (100) *with second-nearest-neighbor interaction*

This solid is sc with nearest-neighbor and second-nearest-neighbor interactions, both with identical spring constant $k$. At zero pressure, the forces between neighbors all vanish, so the spring constants for bond rotations $k^{\perp} = 0$. The crystal is oriented with the (100), (010), and (001) directions along the $x$, $y$, and $z$ axes, respectively. Since the second-nearest neighbors lie in the same plane as nearest neighbors, a single atom unit cell and boundary layer can be used. There are four nearest and four second-nearest neighbors in each layer and one nearest and four second-nearest neighbors in layers above and below. Summing contributions over these neighbors, one finds that the dynamical matrices for this system are given by

$$\mathbf{U}(\vec{q}) = k \begin{pmatrix} 6 - 2c_x(1 + c_y) & 2s_x s_y & 0 \\ 2s_x s_y & 6 - 2(1 + c_x)c_y & 0 \\ 0 & 0 & 6 \end{pmatrix}, \quad \text{(A7)}$$

$$\mathbf{U}_0(\vec{q}) = k \begin{pmatrix} 5 - 2c_x(1 + c_y) & 2s_x s_y & 0 \\ 2s_x s_y & 5 - 2(1 + c_x)c_y & 0 \\ 0 & 0 & 3 \end{pmatrix}, \quad \text{(A8)}$$

$$\mathbf{V}(\vec{q}) = k \begin{pmatrix} -c_x & 0 & is_x \\ 0 & -c_y & is_y \\ is_x & is_y & -1 - c_x - c_y \end{pmatrix}. \quad \text{(A9)}$$

From these expressions we obtain a Green's function that is identical to the analytic expression of Saito.[30]

For this solid the explicit forms of the acoustic sum rule[40] in the bulk and at the surface are

$$\mathbf{V}^{\dagger}(\mathbf{\Gamma}) + \mathbf{U}(\mathbf{\Gamma}) + \mathbf{V}(\mathbf{\Gamma}) = 0, \quad \text{(A10)}$$

$$\mathbf{U}_0(\mathbf{\Gamma}) + \mathbf{V}(\mathbf{\Gamma}) = 0. \quad \text{(A11)}$$

Equations (A7) to (A9) fulfill these rules.

#### *2. fcc* (100) *with nearest-neighbor interaction*

The fcc crystal is oriented with the (110), (1$\bar{1}$0), and (001) directions along the $x$, $y$, and $z$ axes, respectively. This orients the axes along the nearest-neighbor directions and we use the single atom, square unit cell shown in Fig. 1(b). There are four nearest neighbors in the same plane and four in each adjacent layer. The translation vector connecting neighboring layers is $\vec{c} = d_{\mathrm{nn}}(1/2, 1/2, 1/\sqrt{2})$, so successive layers are offset in the $x$-$y$ plane.

We consider the case $k^{\perp} \neq 0$ to allow for cases where the reference state is under pressure. The intralayer force-constant matrix for this lattice is written as $\mathbf{U} = k_{\mathrm{nn}}\mathbf{U}_{\mathrm{nn}}^{\parallel} + k_{\mathrm{nn}}^{\perp}\mathbf{U}_{\mathrm{nn}}^{\perp}$ with the subscript $nn$ denoting nearest neighbors. Then

$$\mathbf{U}_{\mathrm{nn}}^{\parallel}(\vec{q}) = \begin{pmatrix} 4 - 2c_x & 0 & 0 \\ 0 & 4 - 2c_y & 0 \\ 0 & 0 & 4 \end{pmatrix}, \quad \text{(A12)}$$

$$\mathbf{U}_{\mathrm{nn}}^{\perp}(\vec{q}) = \begin{pmatrix} 8 - 2c_y & 0 & 0 \\ 0 & 8 - 2c_x & 0 \\ 0 & 0 & 8 - 2c_x - 2c_y \end{pmatrix}, \quad \text{(A13)}$$

in the bulk and $\mathbf{U}_0 = k_{\mathrm{nn}}\mathbf{U}_0^{\parallel}(\vec{q}) + k_{\mathrm{nn}}^{\perp}\mathbf{U}_0^{\perp}(\vec{q})$ with

$$\mathbf{U}_0^{\parallel}(\vec{q}) = \mathbf{U}_{\mathrm{nn}}^{\parallel}(\vec{q}) - \begin{pmatrix} 1 & 0 & 0 \\ 0 & 1 & 0 \\ 0 & 0 & 2 \end{pmatrix}, \quad \text{(A14)}$$

$$\mathbf{U}_0^{\perp}(\vec{q}) = \mathbf{U}_{\mathrm{nn}}^{\perp}(\vec{q}) - \begin{pmatrix} 3 & 0 & 0 \\ 0 & 3 & 0 \\ 0 & 0 & 2 \end{pmatrix}, \quad \text{(A15)}$$

at the surface. The interlayer force-constant matrix is $\mathbf{V} = (k_{\mathrm{nn}}\mathbf{V}_{\mathrm{nn}}^{\parallel} + k_{\mathrm{nn}}^{\perp}\mathbf{V}_{\mathrm{nn}}^{\perp}) \exp\{i(q_x + q_y)d_{\mathrm{nn}}/2\}$ with

$$\mathbf{V}_{\mathrm{nn}}^{\parallel} = \begin{pmatrix} -c_{\frac{x}{2}}c_{\frac{y}{2}} & s_{\frac{x}{2}}s_{\frac{y}{2}} & i\sqrt{2}s_{\frac{x}{2}}c_{\frac{y}{2}} \\ s_{\frac{x}{2}}s_{\frac{y}{2}} & -c_{\frac{x}{2}}c_{\frac{y}{2}} & i\sqrt{2}c_{\frac{x}{2}}s_{\frac{y}{2}} \\ i\sqrt{2}s_{\frac{x}{2}}c_{\frac{y}{2}} & i\sqrt{2}c_{\frac{x}{2}}s_{\frac{y}{2}} & -2c_{\frac{x}{2}}c_{\frac{y}{2}} \end{pmatrix}, \quad \text{(A16)}$$

$$\mathbf{V}_{\mathrm{nn}}^{\perp} = \begin{pmatrix} -3c_{\frac{x}{2}}c_{\frac{y}{2}} & -s_{\frac{x}{2}}s_{\frac{y}{2}} & -i\sqrt{2}s_{\frac{x}{2}}c_{\frac{y}{2}} \\ -s_{\frac{x}{2}}s_{\frac{y}{2}} & -3c_{\frac{x}{2}}c_{\frac{y}{2}} & -i\sqrt{2}c_{\frac{x}{2}}s_{\frac{y}{2}} \\ -i\sqrt{2}s_{\frac{x}{2}}c_{\frac{y}{2}} & -i\sqrt{2}c_{\frac{x}{2}}s_{\frac{y}{2}} & -2c_{\frac{x}{2}}c_{\frac{y}{2}} \end{pmatrix}. \quad \text{(A17)}$$

Equations (A12) to (A17) fulfill the sum rules Eqs. (A10) and (A11).

#### *3. fcc* (100) *with second-nearest-neighbor interaction*

For the discussion of second-nearest-neighbor interactions we use the same unit cell within the surface plane but must increase the width of the boundary layer to two atomic planes so $n_c = 2$. Successive layers are not offset so the translation vector is perpendicular to the plane: $\vec{c} = d_{\mathrm{nn}}(0, 0, \sqrt{2})$. There are four second-nearest neighbors in the same plane, and one in each layer with distance $2d_{\mathrm{nn}}$. The vectors and matrices in Sec. II all have dimension $3n_c$, but it is useful to divide them into terms associated with each atom. The displacements and forces are then expressed as $n_c$ vectors of length 3 or $n_c \times n_c$ arrays of $3 \times 3$ matrices. Using tildes to identify smaller $3 \times 3$ matrices, the force-constant matrix elements become

$$\mathbf{U_0} = \begin{pmatrix} \tilde{\mathbf{U}}_{\mathbf{0}} & \tilde{\mathbf{V}}e^{i(q_x+q_y)d_{\mathrm{nn}}/2} \\ \tilde{\mathbf{V}}^{\dagger}e^{-i(q_x+q_y)d_{\mathrm{nn}}/2} & \tilde{\mathbf{U}}_1 \end{pmatrix}, \quad \text{(A18)}$$

$$\mathbf{U} = \begin{pmatrix} \tilde{\mathbf{U}} & \tilde{\mathbf{V}}e^{i(q_x+q_y)d_{\mathrm{nn}}/2} \\ \tilde{\mathbf{V}}^{\dagger}e^{-i(q_x+q_y)d_{\mathrm{nn}}/2} & \tilde{\mathbf{U}} \end{pmatrix}, \quad \text{(A19)}$$

$$\mathbf{V} = \begin{pmatrix} \tilde{\mathbf{W}} & \mathbf{0} \\ \tilde{\mathbf{V}} e^{-i(q_x+q_y)/2} & \tilde{\mathbf{W}} \end{pmatrix}. \tag{A20}$$

In the following, $k_{\rm nn}^{\parallel}$ and $k_{\rm 2n}^{\parallel}$ are the spring constants for nearest-neighbor and second-nearest-neighbor bond stretching, while $k_{\rm nn}^{\perp}$ and $k_{\rm 2n}^{\perp}$ are the spring constants for first- and second-nearest-neighbor bond rotation, respectively. The intralayer force-constant matrix is given by $\tilde{\mathbf{U}} = \tilde{\mathbf{U}}_{\rm nn} + \tilde{\mathbf{U}}_{\rm 2n}$ with $\tilde{\mathbf{U}}_{\rm nn} = k_{\rm nn}^{\parallel}\tilde{\mathbf{U}}_{\rm nn}^{\parallel} + k_{\rm nn}^{\perp}\tilde{\mathbf{U}}_{\rm nn}^{\perp}$ and $\tilde{\mathbf{U}}_{\rm 2n} = k_{\rm 2n}^{\parallel}\tilde{\mathbf{U}}_{\rm 2n}^{\parallel} + k_{\rm 2n}^{\perp}\tilde{\mathbf{U}}_{\rm 2n}^{\perp}$. The expressions for $\tilde{\mathbf{U}}_{\rm nn}^{\parallel}$ and $\tilde{\mathbf{U}}_{\rm nn}^{\perp}$ are identical to the nearest-neighbor fcc (100) case and given in Eqs. (A12) and (A13). The contribution due to second-nearest neighbors is

$$\tilde{\mathbf{U}}_{\rm 2n}^{\parallel}(\vec{q}) = \begin{pmatrix} 2-2c_xc_y & 2s_xs_y & 0 \\ 2s_xs_y & 2-2c_xc_y & 0 \\ 0 & 0 & 2 \end{pmatrix}, \tag{A21}$$

$$\tilde{\mathbf{U}}_{\rm 2n}^{\perp}(\vec{q}) = \begin{pmatrix} 4-2c_xc_y & -2s_xs_y & 0 \\ -2s_xs_y & 4-2c_xc_y & 0 \\ 0 & 0 & 4-4c_xc_y \end{pmatrix}. \tag{A22}$$

In this case, the surface force-constant matrix element becomes $\tilde{\mathbf{U}}_0 = \tilde{\mathbf{U}}_0^{\parallel} + \tilde{\mathbf{U}}_0^{\perp}$ with

$$\tilde{\mathbf{U}}_0^{\parallel}(\vec{q}) = k_{\rm nn}^{\parallel}\left\{\tilde{\mathbf{U}}_{\rm nn}^{\parallel}(\vec{q}) - \begin{pmatrix} 1&0&0\\0&1&0\\0&0&2\end{pmatrix}\right\} + k_{\rm 2n}^{\parallel}\left\{\tilde{\mathbf{U}}_{\rm 2n}^{\parallel}(\vec{q}) - \begin{pmatrix} 0&0&0\\0&0&0\\0&0&1\end{pmatrix}\right\}, \tag{A23}$$

$$\tilde{\mathbf{U}}_1^{\parallel}(\vec{q}) = k_{\rm nn}^{\parallel}\tilde{\mathbf{U}}_{\rm nn}^{\parallel}(\vec{q}) + k_{\rm 2n}^{\parallel}\left\{\tilde{\mathbf{U}}_{\rm 2n}^{\parallel}(\vec{q}) - \begin{pmatrix} 0&0&0\\0&0&0\\0&0&1\end{pmatrix}\right\}, \tag{A24}$$

$$\tilde{\mathbf{U}}_0^{\perp}(\vec{q}) = k_{\rm nn}^{\perp}\left\{\tilde{\mathbf{U}}_{\rm nn}^{\perp}(\vec{q}) - \begin{pmatrix} 3&0&0\\0&3&0\\0&0&2\end{pmatrix}\right\} + k_{\rm 2n}^{\perp}\left\{\mathbf{U}_{\rm 2n}^{\perp}(\vec{q}) - \begin{pmatrix} 1&0&0\\0&1&0\\0&0&0\end{pmatrix}\right\}, \tag{A25}$$

$$\tilde{\mathbf{U}}_1^{\perp}(\vec{q}) = k_{\rm nn}^{\perp}\tilde{\mathbf{U}}_{\rm nn}^{\perp}(\vec{q}) + k_{\rm 2n}^{\perp}\left\{\tilde{\mathbf{U}}_{\rm 2n}^{\perp}(\vec{q}) - \begin{pmatrix} 1&0&0\\0&1&0\\0&0&0\end{pmatrix}\right\}, \tag{A26}$$

while the interlayer force-constant matrices are

$$\tilde{\mathbf{V}}^{\parallel}(\vec{q}) = k_{\rm nn}^{\parallel}\tilde{\mathbf{V}}_{\rm nn}^{\parallel}(\vec{q}), \tag{A27}$$

$$\tilde{\mathbf{V}}^{\perp}(\vec{q}) = k_{\rm nn}^{\perp}\tilde{\mathbf{V}}_{\rm nn}^{\perp}(\vec{q}), \tag{A28}$$

$$\tilde{\mathbf{W}}^{\parallel}(\vec{q}) = k_{\rm 2n}^{\parallel}\begin{pmatrix} 0&0&0\\0&0&0\\0&0&-1\end{pmatrix}, \tag{A29}$$

$$\tilde{\mathbf{W}}^{\perp}(\vec{q}) = k_{\rm 2n}^{\perp}\begin{pmatrix} -1&0&0\\0&-1&0\\0&0&0\end{pmatrix}. \tag{A30}$$

The expressions for $\tilde{\mathbf{V}}_{\rm nn}^{\parallel}$ and $\tilde{\mathbf{V}}_{\rm nn}^{\perp}$ are identical to the nearest-neighbor fcc (100) case given in Eqs. (A16) and (A17).

For second-nearest-neighbor interactions the acoustic sum rules become

$$\tilde{\mathbf{W}}^{\dagger}(\mathbf{\Gamma}) + \tilde{\mathbf{V}}^{\dagger}(\mathbf{\Gamma}) + \tilde{\mathbf{U}}(\mathbf{\Gamma}) + \tilde{\mathbf{V}}(\mathbf{\Gamma}) + \tilde{\mathbf{W}}(\mathbf{\Gamma}) = 0, \tag{A31}$$

$$\tilde{\mathbf{V}}^{\dagger}(\mathbf{\Gamma}) + \tilde{\mathbf{U}}_1(\mathbf{\Gamma}) + \tilde{\mathbf{V}}(\mathbf{\Gamma}) + \tilde{\mathbf{W}}(\mathbf{\Gamma}) = 0, \tag{A32}$$

$$\tilde{\mathbf{U}}_0(\mathbf{\Gamma}) + \tilde{\mathbf{V}}(\mathbf{\Gamma}) + \tilde{\mathbf{W}}(\mathbf{\Gamma}) = 0. \tag{A33}$$

It is straightforward to check that these are fulfilled by Eqs. (A21) to (A30).

The values for the individual spring constants are evaluated from the derivatives of the potential at the equilibrium spacing. Here we use the Lennard-Jones potential given by Eq. (34) for $r < r_1$ and smoothly spline it to zero force between $r_1 = 1.35\sigma$ and $r_2 = 1.8\sigma$. Evaluating the derivatives for the zero-pressure equilibrium state yields $k_{\rm nn}^{\parallel} = 65.6\frac{\epsilon}{\sigma^2}$, $k_{\rm 2n}^{\parallel} = -5.06\frac{\epsilon}{\sigma^2}$, $k_{\rm nn}^{\perp} = -0.41\frac{\epsilon}{\sigma^2}$, and $k_{\rm 2n}^{\perp} = 0.41\frac{\epsilon}{\sigma^2}$. The force $\vec{f}_0$ is has magnitude $F_0 = 0.64\frac{\epsilon}{\sigma}$ at the boundary layer and is directed away from the bulk at the top layer of atoms and toward the bulk at the bottom layer: $\vec{f}_0 = (0,0,F_0,0,0,-F_0)$ [see also Eq. (5) in Sec. II].

## APPENDIX B: ISOTROPIC CONTINUUM ELASTICITY

For completeness, we compare the surface stiffness coefficients to the behavior of $\mathbf{\Phi}(\vec{q}) = \mathbf{G}^{-1}(\vec{q})$ for a purely continuum elastic media. The solution is obtained by a Fourier analysis of the equations for mechanical equilibrium in continuous isotropic elastic bodies[21,22,65] and reads

$$\mu\mathbf{G}(\vec{q}) = \begin{pmatrix} \frac{1}{q} - \frac{\nu q_x^2}{q^3} & -\frac{\nu q_x q_y}{q^3} & i\frac{(1-2\nu)q_x}{2q^2} \\ -\frac{\nu q_x q_y}{q^3} & \frac{1}{q} - \frac{\nu q_y^2}{q^3} & i\frac{(1-2\nu)q_y}{2q^2} \\ -i\frac{(1-2\nu)q_x}{2q^2} & -i\frac{(1-2\nu)q_y}{2q^2} & \frac{1-\nu}{q} \end{pmatrix}, \tag{B1}$$

where $\mu$ is the shear modulus and $\nu$ Poisson's ratio. All calculations reported here are for $\nu = 0$. A continuous medium has complete translational symmetry and the BZ extends over all $q$. However, we only specify displacements at the discrete set of surface atoms and use the corresponding BZ. This is similar to approximating the continuum equations by solving on a discrete mesh.

*lars.pastewka@iwm.fraunhofer.de
†mr@pha.jhu.edu

[1] B. Luan and M. O. Robbins, Nature **435**, 929 (2005).
[2] R. W. Carpick, D. F. Ogletree, and M. Salmeron, J. Colloid Interf. Sci. **211**, 395 (1999).
[3] S. Akarapu, T. Sharp, and M. O. Robbins, Phys. Rev. Lett. **106**, 204301 (2011).
[4] C. Campañá, B. N. J. Persson, and M. H. Müser, J. Phys.: Condens. Matter **23**, 085001 (2011).
[5] J. R. Kermode, T. Albaret, D. Sherman, N. Bernstein, P. Gumbsch, M. C. Payne, G. Csányi, and A. de Vita, Nature **455**, 1224 (2008).
[6] S. Kohlhoff, P. Gumbsch, and H. F. Fischmeister, Philos. Mag. A **64**, 851 (1991).
[7] G. Moras, L. C. Ciacchi, C. Elsässer, P. Gumbsch, and A. de Vita, Phys. Rev. Lett. **105**, 075502 (2010).
[8] V. Shchukin and D. Bimberg, Rev. Mod. Phys. **71**, 1125 (1999).
[9] R. E. Miller and E. B. Tadmor, Modelling Simul. Mater. Sci. Eng. **17**, 053001 (2009).
[10] A. Ramasubramaniam and E. A. Carter, MRS Bull. **32**, 913 (2007).
[11] R. E. Miller and E. B. Tadmor, MRS Bull. **32**, 920 (2007).
[12] V. B. Shenoy, R. Miller, E. B. Tadmor, R. Phillips, and M. Ortiz, J. Mech. Phys. Solids **47**, 611 (1999).
[13] K. Ohsawa, E. Kuramoto, and T. Suzuki, Philos. Mag. A **74**, 431 (1996).
[14] V. K. Tewary and R. Thomson, J. Mater. Res. **7**, 1018 (1992).
[15] R. Thomson, S. J. Zhou, A. E. Carlsson, and V. K. Tewary, Phys. Rev. B **46**, 10613 (1992).
[16] V. K. Tewary, Adv. Phys. **22**, 757 (1973).
[17] A. A. Maradudin, E. W. Montroll, G. H. Weiss, and I. P. Ipatova, *Theory of Lattice Dynamics in the Harmonic Approximation*, 2nd ed., edited by H. Ehrenreich, F. Seitz, and D. Turnbull (Academic, New York, 1976).
[18] D. T. Read and V. K. Tewary, Nanotechnology **18**, 105402 (2007).
[19] V. K. Tewary and D. T. Read, Comp. Model. Eng. Sci. **6**, 359 (2004).
[20] V. K. Tewary, Phys. Rev. B **69**, 094109 (2004).
[21] S. Barbot and Y. Fialko, Geophys. J. Int. **182**, 568 (2010).
[22] C. L. Amba-Rao, J. Frankl. Inst. **287**, 241 (1969).
[23] I. N. Sneddon, Int. J. Eng. Sci. **3**, 47 (1965).
[24] M. Ghazisaeidi and D. R. Trinkle, Phys. Rev. B **82**, 064115 (2010).
[25] C. Campañá and M. H. Müser, Phys. Rev. B **74**, 075420 (2006).
[26] W. Cai, M. de Koning, V. V. Bulatov, and S. Yip, Phys. Rev. Lett. **85**, 3213 (2000).
[27] C. Campañá, Phys. Rev. E **78**, 026110 (2008).
[28] C. Campañá, M. H. Müser, and M. O. Robbins, J. Phys.: Condens. Matter **20**, 354013 (2008).
[29] C. Campañá and M. H. Müser, Europhys. Lett. **77**, 38005 (2007).
[30] Y. Saito, J. Phys. Soc. Jpn. **73**, 1816 (2004).
[31] W. B. Dapp, A. Lücke, B. N. J. Persson, and M. H. Müser, Phys. Rev. Lett. **108**, 244301 (2012).
[32] S. J. Plimpton and A. P. Thompson, MRS Bull. **37**, 513 (2012).
[33] L. T. Kong, G. Bartels, C. Campañá, C. Denniston, and M. H. Müser, Comput. Phys. Commun. **180**, 1004 (2009).
[34] S. Plimpton, J. Comput. Phys. **117**, 1 (1995).
[35] The dissipation in bulk solids is typically proportional to some power of the three-dimensional wave vector $\vec{q}$. The modes at the $\Gamma$ point of the two-dimensional Brillouin zone of the surface will have a nonzero normal component $q_z$ of this wave vector. This is the reason collective surface excitations decay at all. Their relaxation time is, however, long and diverges as $q_z \to 0$.
[36] L. M. Falicov and F. Ynduráin, J. Phys. C: Solid State Phys. **8**, 147 (1975).
[37] V. R. Velasco and F. Ynduráin, Surf. Sci. **85**, 107 (1979).
[38] M. O. Robbins and B. Koiller, Phys. Rev. B **32**, 4576 (1985).
[39] C. E. T. Gonçalves da Silva and B. Koiller, Solid State Commun. **40**, 215 (1981).
[40] N. W. Ashcroft and N. D. Mermim, *Solid State Physics* (Thomson Learning, London, UK, 1976).
[41] R. P. Gupta, Phys. Rev. B **23**, 6265 (1981).
[42] K. Huang, *Statistical Mechanics* (Wiley, New York, 1987).
[43] L. Onsager, Phys. Rev. **65**, 117 (1944).
[44] E. Ising, Z. Phys. **31**, 253 (1925).
[45] K. L. Johnson, *Contact Mechanics* (Cambridge University Press, Cambridge, UK, 1985).
[46] M. E. Peskin and D. V. Schroeder, *An Introduction to Quantum Field Theory* (Westview Press, Boulder, CO, 1995).
[47] This potential is implemented as `lj/smooth` in LAMMPS.[32,34]
[48] H. Hertz, J. reine angew. Math. **92**, 156 (1881).
[49] J. J. Vlassak and W. D. Nix, J. Mech. Phys. Solids **42**, 1223 (1994).
[50] J. J. Vlassak and W. D. Nix, Philos. Mag. A **67**, 1045 (1993).
[51] S. Cheng and M. O. Robbins, Tribol. Lett. **39**, 329 (2010).
[52] M. T. Knippenberg, P. T. Mikulski, and J. A. Harrison, Modelling Simul. Mater. Sci. Eng. **18**, 034002 (2010).
[53] B. Luan and M. O. Robbins, Phys. Rev. E **74**, 026111 (2006).
[54] P. Meakin, *Fractals, Scaling and Growth Far from Equilibrium* (Cambridge University Press, Cambridge, UK, 1998).
[55] C. Putignano, L. Afferrante, G. Carbone, and G. Demelio, J. Mech. Phys. Solids **60**, 973 (2012).
[56] S. Hyun, L. Pei, J. F. Molinari, and M. O. Robbins, Phys. Rev. E **70**, 026117 (2004).
[57] H. Tsuzuki, P. S. Branicio, and J. P. Rino, Comput. Phys. Commun. **177**, 518 (2007).
[58] J. D. Honeycutt and H. C. Andersen, J. Phys. Chem. **91**, 4950 (1987).
[59] G. Anciaux and J.-F. Molinari, Int. J. Numer. Meth. Eng. **79**, 1041 (2009).
[60] L. E. Shilkrot, R. E. Miller, and W. A. Curtin, Phys. Rev. Lett. **89**, 025501 (2002).
[61] S. M. Foiles and M. I. Baskes, MRS Bull. **37**, 485 (2012).
[62] L. Pastewka, M. Mrovec, M. Moseler, and P. Gumbsch, MRS Bull. **37**, 493 (2012).
[63] E. Tadmor, F. Legoll, W. K. Kim, L. M. Dupuy, and R. E. Miller, Appl. Mech. Rev. (in press).
[64] L. M. Dupuy, E. B. Tadmor, R. E. Miller, and R. Phillips, Phys. Rev. Lett. **95**, 060202 (2005).
[65] L. D. Landau and E. M. Lifshitz, *Theory of Elasticity* (Butterworth-Heinemann, Oxford, UK, 1986).